Journal of Alloys and Compounds, 553 (2013) 119-124
http://dx.doi.org/10.1016/j.jallcom.2012.11.099

Role of starting phase of boron on the mechanical alloying of FeNbB composition

J.J. Ipus[1], J.S. Blázquez[1*], V. Franco[1], S. Lozano-Pérez[2], A. Conde[1]

[1]Dpto. Física de la Materia Condensada, ICMSE-CSIC, Universidad de Sevilla, P.O. Box 1065, 41080, Sevilla, Spain.

[2]University of Oxford, Parks Road, Oxford OX1 P3H, UK.

Abstract

Mechanical alloyed $Fe_{75}Nb_{10}B_{15}$ systems, prepared with crystalline or commercial amorphous boron and a similar composition with the same Fe/Nb ratio but no boron, have been studied as a function of milling time in the aim of enhancing the homogenization of boron and determining its role on the mechanical alloying process. Neither boron addition nor boron phase used affect the developed microstructure at very early stages. After 4 h milling at 350 rpm, the formation of an amorphous phase was observed for boron containing compositions while for the boron-free alloy a supersaturated solid solution was found in the final microstructure. The alloy prepared using commercial amorphous boron showed a larger fraction of amorphous phase than that prepared using crystalline boron for the same milling time, suggesting that amorphous boron accelerates the formation of the amorphous phase during mechanical alloying.

[*]Corresponding author: J.S. Blázquez

Phone: (34) 954556029/Fax: (34) 954612097

E-mail:jsebas@us.es

Journal of Alloys and Compounds, 553 (2013) 119-124
http://dx.doi.org/10.1016/j.jallcom.2012.11.099

Introduction

Fe-based amorphous and nanocrystalline alloys are very interesting materials due to their improved magnetic properties, which can be strongly enhanced with respect to those exhibited by conventional microstructures [1]. Nanocrystalline Fe-M-B type alloys, so called Nanoperm [2] (M is an early transition metal), have been attractive for their excellent soft magnetic properties and are used as ultrasoft magnets in several commercial applications [1,3]. These good soft magnetic properties depend on the microstructure of material [4,5] and thus the microstructural characterization is very important in order to understand the physical behavior of the system and to predict its possible technological capabilities.

Although these systems are generally obtained by rapid quenching and subsequent annealing, nanocrystalline alloys of these compositions can be directly obtained by mechanical alloying from elemental powders. The former method assures a good homogenization of the precursor amorphous alloy as the starting point is a liquid. However, using mechanical alloying from elemental powders, hard materials can be retained as inclusions in a matrix formed by more ductile materials [6]. This fact implies a different composition of the matrix than that expected for a homogeneous mixture. Boron is an element widely used in glassy alloys as it enhances the glass forming ability of the Fe-based alloys. However, crystalline boron is a very hard material and thus a good homogeneization of this element via mechanical alloying is not straightforward. In a previous study we have described the microstructural evolution with milling time of a $Fe_{75}Nb_{10}B_{15}$ alloy prepared using crystalline boron in the starting mixture [7] and almost pure boron inclusions were found embedded in an amorphous matrix [8] even after long milling times.

Journal of Alloys and Compounds, 553 (2013) 119-124
http://dx.doi.org/10.1016/j.jallcom.2012.11.099

In this work we prepared a $Fe_{75}Nb_{10}B_{15}$ alloy using commercial amorphous boron instead of crystalline one in the starting mixture. Another alloy with the same Fe/Nb ratio but no boron was also prepared. The study of these alloys could help us to elucidate the role of boron and its initial phase in the microstructural evolution as milling progresses (e.g, dissolution of B and Nb atoms into Fe lattice and amorphous phase, formation of amorphous phase or other phases, etc.)

Experimental

Two $Fe_{75}Nb_{10}B_{15}$ alloys, using crystalline (c-B alloy) and commercial amorphous boron (a-B alloy) and a third alloy without boron (n-B), with the same Fe/Nb ratio, were prepared using commercial amorphous (95-97% purity) and crystalline boron (≥99 % purity) powders, along with Fe and Nb powders (≥99 % purity) from ChemPur chemical supplier. Alloying was performed by milling using the elemental powders as starting materials in a planetary mill Fritsch Pulverisette 4 Vario, with steel balls (10 mm diameter) and hardened steel vials (250 cm^3), initial powder mass of 30 g and a ball to powder ratio of 10:1. The rotational speed of the disc which supports the vials was 350 rpm and that of the vials was 700 rpm in opposite direction. After selected milling times, some powder was taken out from the vials to characterize its microstructure as a function of the milling time. Opening and closing of vials were done under Ar atmosphere in a Saffron Omega glove box to avoid oxygen and humidity contamination.

Phases present and microstructure were studied by X-ray diffraction (XRD), using Cu Kα radiation in a Bruker D8I diffractometer and the local environment of Fe atoms was analyzed by Mössbauer spectrometry. Figure 1 shows the XRD patterns of

both initial boron powders. It can be seen that the crystalline boron has a rhombohedral ($R\bar{3}m$) phase with lattice parameters a = b = 10.925 Å and c= 23.814 Å. However, the commercial amorphous boron powder shows a tri-phased structure with ~50% amorphous phase, being the rest rhombohedral boron-phase and a borane nitride azide type phase $(N_3)(NB_9H_{11})$. Mössbauer spectra were recorded at room temperature in a transmission geometry using a ^{57}Co(Rh) source. The values of the hyperfine parameters were obtained by fitting with NORMOS program [9] and the isomer shift (IS) was quoted relative to that of α-Fe at room temperature. Thermal characterization of the samples was studied by differential scanning calorimetry (DSC) using a Perkin-Elmer DSC7 in Ar atmosphere.

Local microstructure was studied by scanning transmission electron microscopy (STEM) using a Jeol JEM3000F microscope operated at 297 kV. STEM mode was used to obtain high-angle annular dark field (HAADF) images and selected area electron diffraction (SAED) patterns were used to identify the phases present. Chemical analysis was performed by energy dispersive X-ray spectroscopy (EDX) for Fe, Nb and Cr (for contamination), using an Oxford Instruments EDS ultra-thin window detector running Inca software. Electron energy loss spectroscopy (EELS) was used for boron with a Gatan image filter (GIF) 2002, which provided an energy resolution of ~1 eV. Sample preparation was performed by focused ion beam (FIB), using a FEI 200 and a Zeiss NVision 40, following the lift out procedure [10], applied to individual powder particles [8].

Results

Phase evolution as a function of milling time for all compositions is shown in figure 2 for selected times. For short milling times, t≤ 3 h, the diffraction peaks from

Journal of Alloys and Compounds, 553 (2013) 119-124
http://dx.doi.org/10.1016/j.jallcom.2012.11.099

bcc-Fe and bcc-Nb phases can be clearly detected for all samples. Moreover, we see a continuous broadening of the (110) diffraction peak of the α-Fe phase for all the alloys which could be related to an increase of microstrains and a decrease in the crystal size. After 3 h milling, while the full width at half maximum reaches a stable value for boron free composition, a continuous increase of the full width at half maximum is found for boron containing alloys.

After 4 h milling, the diffraction peaks from Nb phase are no longer detected for any alloy. We can follow the evolution of the Nb phase as a function of milling time, representing the fraction of bcc-Nb phase measured as:

$$X_{Nb} = \frac{f_{Nb} A_{Nb}}{f_{Nb} A_{Nb} + f_{Fe} A_{Fe}} \quad (1)$$

where A_{Fe} and A_{Nb} correspond to the area of the (110) diffraction peak of the corresponding phases and f_{Fe} and f_{Nb} are the atomic scattering factors of Fe or Nb atoms. In this approximation we neglect the presence of Nb in the bcc-Fe phase although mean scattering power must change after dissolution of some Nb atoms into the Fe lattice. Figure 3 shows the fraction of bcc-Nb phase as a function of milling time, where we can see that at 0.5 h milling all alloys show around 12 % of bcc-Nb phase, close to the nominal value. For longer milling times we can see an approximately constant rate of reduction for the Nb phase fraction with the milling time for all compositions (-4.1 ±0.3, -4.2 ±0.2 and -3.6 ±0.2 %/h for n-B, c-B and a-B, respectively). However, the a-B alloy still presents a small amount of Nb phase (~3 %) at 3.5 h when c-B and n-B alloys do not show any.

After milling for t= 4 h, we can see an important shift to low angles in the position of the (110) α-Fe diffraction peak, related to the incorporation of Nb into the

Journal of Alloys and Compounds, 553 (2013) 119-124
http://dx.doi.org/10.1016/j.jallcom.2012.11.099

bcc-Fe lattice and thus the formation of a supersaturated solid solution for all compositions. For longer milling times, t> 6 h, the formation of an amorphous halo centered at 2θ~ 44º in the diffraction patterns can be observed only for the two boron containing alloys, while for boron free composition the solid solution is the final microstructure.

The evolution of the different local Fe environments with the milling time for each composition can be followed by Mössbauer spectrometry. Figure 4 shows Mössbauer spectra for some selected milling times. For 0.5 h milling a single contribution with a hyperfine field HF= 33 T is observed for all compositions, which corresponds to pure bcc-Fe sites. After this time, new Fe environments with a hyperfine field lower than 33 T appear, associated with new Fe neighborhoods. These Fe rich environments can be related either to Fe atoms in the α-Fe phase but in the presence of impurities or Fe atoms at the interface region of nanocrystals [11].

Other kind of Fe neighborhoods with a negligible hyperfine field, HF≤ 5T, associated with Nb rich environments are also formed after t= 0.5 h milling. The Fe fraction in these sites initially increases with milling time for all alloys up to 4 h milling. However, after 4 h milling, whereas this fraction increases significantly for boron containing alloys (even becoming the dominant Fe environment at the end of the milling), in the case of n-B alloy, the Fe fraction from these sites reaches a maximum value at t= 4 h and then reduces to a stable value after t= 10 h milling.

Figure 5 shows a HAADF image and two SAED patterns from a a-B sample after 40 h milling. The image mainly shows an amorphous microstructure confirmed by the SAED pattern shown in figure 5b. Moreover, there are some dark regions (interpreted as light element inclusions, as HAADF gives us compositional contrast)

Journal of Alloys and Compounds, 553 (2013) 119-124
http://dx.doi.org/10.1016/j.jallcom.2012.11.099

dispersed on the amorphous matrix. A SAED pattern taken on one of these regions is shown in figure 5c and confirms that these dark zones correspond to crystalline inclusions. A plausible indexation for figure 5c is β-boron in a [110] zone axis, which matches with the crystalline phase detected in the initial boron powder.

EDX (for Fe, Nb and Cr) and EELS (for B) compositional profiles taken through a line that crosses one of these crystalline inclusions are shown in figure 6 and reveal that they correspond to boron rich inclusions. In fact, these crystalline B inclusions have been previously observed in the case of c-B samples [8]. The detection of these crystalline inclusions for the a-B sample could be related to the crystalline boron fraction detected in the initial commercial amorphous boron powder, which is not efficiently alloyed in the milling process. Spot EELS spectra on the amorphous matrix and on a boron inclusion, confirmed the presence of the dissolved boron in the matrix (see figure 7, where the boron K-edge is shown for the two areas).

Figure 8 shows the DSC scans of different as-milled samples taken at a heating rate of 40 K/min for boron containing alloys. For all milling times a broad exothermic peak starting at ~700 K can be seen for both alloys, possibly related with a microstructural relaxation, crystal growth [7] and/or phase stabilization. For milling times longer than 10 h a second peak can be observed, ascribed to crystallization of the amorphous phase. We can see that the DSC peak temperature of this process (table 1) shifts to lower temperatures as milling progresses for both alloys and, for a given milling time, these values are also lower for a-B alloy than those for c-B alloy. This trend is also observed for the peak temperature corresponding to the broad exothermic process. It is worth noticing the presence of an endothermic peak at ~620 K for 4 and 6 h milling in the case of a-B alloy. Unlike for c-B alloy, this process is ascribed to the

fusion of an intermetallic phase and has been observed for mechanical alloyed FeGeNb compound [12].

Discussion

In order to extract information from the XRD patterns, a deconvolution procedure was applied to resolve the overlapping of the amorphous and crystalline contributions. A Lorentzian profile to simulate the crystalline peak and a Gaussian profile to simulate the amorphous halo were used to fit the patterns. The crystalline volume fraction was calculated from the area ratio between the crystalline and amorphous plus crystalline contributions.

From the position of the (110) α-Fe we have calculated the evolution of lattice parameter, *a*, for this phase as is shown in figure 9a. It can be seen that the lattice parameter follows the same trend for all alloys up to 4 h milling, increasing continuously. However, after 2 h milling, the boron free alloy shows a larger value of *a* than the boron containing alloys.

At 4 h milling, when the supersaturated solid solution is formed in all alloys, the lattice parameters are: 2.901 ±0.005 Å, 2.895 ±0.005 Å and 2.890 ±0.005 Å, for n-B, c-B and a-B, alloys respectively. This increase in the lattice parameter could be ascribed to the dissolution of Nb atoms into the Fe lattice, in agreement with the progressive reduction of bcc-Nb phase showed in figure 3. Vegard's law has been used to estimate an amount of ~1 and ~7 at.% of Nb into the α-Fe(Nb) phase at 2 and 4 h, respectively. This would suggest that not all Nb is dissolved inside the bcc-Fe(Nb) lattice, in agreement with the low solubility of this element in the α-Fe lattice. Therefore, Nb enrichment should be expected in the crystal boundary region, even after the formation of the supersaturated solid solution.

For longer milling times, t> 4 h, we can see an almost constant lattice parameter value for boron containing alloys, with an average *a*= 2.898 ±0.005 Å. However, in the n-B alloy, the lattice parameter increases for milling times up to 10 h and then decreases, being always higher than the corresponding one in boron containing alloys. This difference in the lattice parameter could be ascribed to some lattice disorder including interstitials atoms.

The large broadening observed from 0 to 4 h milling in the (110) α-Fe diffraction peak for all alloys can be related to both a refinement of the crystal size and an increase of the microstrains with the milling time. It is worth mentioning that this broadening is higher for boron containing alloys, which could suggest that the boron inclusions, as shown in figure 5a and [8], play the role of an extra milling media helping to reduce the crystal size. This can be observed in figure 9b where the crystal size for boron free alloy is a bit higher, D= 13 nm, than for boron containing alloys, D= 10 and 9 ±1 nm, for c-B and a-B alloys, respectively.

For longer milling times, a constant value of crystal size and microstrains is observed but a higher value of microstrains for c-B alloy with respect to the other alloys is found. In fact, we have showed the presence of crystalline boron inclusions for c-B alloy, suggesting that the amount of these inclusions in the case of a-B alloy is lower and that the higher amount of boron inclusions could rise up the microstrains for c-B alloy.

For milling t= 40 h, the formation of an amorphous phase in boron containing alloys is clearly distinguishable, while for the boron free composition a supersaturated solid solution is the final microstructure developed. In figure 10a we can see the evolution of the crystalline volume fraction as a function of the milling time for boron

containing compositions. It is evident that boron addition is necessary to amorphizise the alloy with the Fe/Nb ratio used. However, binary Fe-Nb compositions with a Nb content ≥30 at.% can be amorphized by milling [13,14,15]. In figure 10 we can see that the use of commercial amorphous or crystalline boron to prepare the starting mixture can lead to different results. In the case of a-B alloy we can see the formation of some amorphous fraction, even after 3 h milling, while for c-B alloy the amorphous phase is only detected by XRD after 6 h milling. As the milling conditions were the same for both alloys, this difference in time evidences that the c-B alloy needs approximately double energy (dose) transferred to the powders from the milling media [16,17] to produce a similar microstructure. The rate at which the crystalline fraction decreases is higher for a-B alloy up to 10 h, which means a faster developing of amorphous phase for this alloy. After 10 h, the amorphization rate is almost the same for both boron containing alloys, leading to a higher amorphous fraction for a-B alloy. Therefore, we can suggest that the incorporation of amorphous boron to the matrix is faster than for crystalline one.

Figure 10b shows the fraction of Fe atoms in the Nb rich environments, HF ≤ 5 T. The use of paramagnetic singlet or doublet contributions or very low hyperfine field contributions in the fitting is ambiguous in complex systems as the one studied here. Therefore, in the current study all contributions with a hyperfine field less than 5 T are considered as paramagnetic contribution. It can be seen that for milling times below 3 h, this low HF Fe fraction increases at the same rate for all the alloys including the n-B alloy, suggesting that the formation of low HF Fe sites is not related to boron addition or the presence of amorphous boron phase but might be ascribed to the presence of Nb atoms in the vicinity of Fe.

For longer milling times, t> 4 h, a continuous increase of Fe fraction in Nb rich environments is observed for a-B and c-B alloys, while for n-B alloy this Fe fraction decreases reaching a stable value after 10 h milling. The Fe fraction is always higher for a-B alloy than for c-B one. Thus, linking this Fe fraction with the formation of the amorphous phase, this result agrees with those found by XRD where a higher amorphous fraction was found for a-B alloy.

Figure 10c shows the IS of the low hyperfine field contributions (HF≤ 5T). This parameter behaves in a similar way for the three studied alloys as a function of milling time, being independent of boron addition. In fact, the minimum IS found can be related to the maximum observed for the Fe fraction in HF≤ 5T sites for the n-B alloy. This behavior is related to the process of Nb homogenization in the alloys. For short milling times, below 3 h, Nb crystals are still detected. As milling progresses, these Nb crystals which are ductile material, are elongated, presenting an increasing surface to the Fe matrix. Therefore, there is a population of Fe atoms facing these elongated crystals, with a high number of Nb in their neighborhood, whereas a large population of Fe atoms shows no significant Nb in their neighborhood (sharp high HF peak in the distributions). As milling progresses further and Nb becomes homogeneous in the matrix, the Nb rich and almost pure Fe environments reduce. As Nb increases in the bcc-Fe, IS decreases -0.03 mm/s per Nb atom in the first shell and -0.02 mm/s per Nb atom in the second shell [18]. Therefore, the minimum IS value observed in Fig.10c indicates the presence of Fe environments very rich in Nb (≥5 Nb atoms as near neighbors and/or next near neighbors) which progressively disappear as milling progresses and Nb diffuses into the matrix.

Journal of Alloys and Compounds, 553 (2013) 119-124
http://dx.doi.org/10.1016/j.jallcom.2012.11.099

Conclusions

We have prepared two $Fe_{75}Nb_{10}B_{15}$ alloys, in order to study the microstructural evolution and the role of boron on their mechanical alloying process. One alloy was prepared using crystalline boron as precursor, and a second one using commercial amorphous boron. A third boron-free alloy was also prepared for comparison.

From the XRD results we find that the addition of boron in the composition leads to a finer crystal size and a smaller lattice parameter than for the boron-free alloy. Moreover, it is observed that for the studied Fe/Nb ratio the addition of boron is needed to form the amorphous phase. Moreover, the use of commercial amorphous boron instead of crystalline one in the starting mixture speeds up the formation of the amorphous phase, developing in a larger fraction for the same milling time.

From Mössbauer spectra we have find the presence of Fe atoms in Nb rich neighborhoods which is related to the amorphous phase detected by XRD. From the evolution of the Fe fraction in these sites it is possible to suggest that, although Nb atoms are responsible for such Fe environments, the boron addition is necessary to increase the Fe fraction in these sites and to develop the amorphous phase.

Acknowledgments

This work was supported by the Spanish Ministry of Science and Innovation (MICINN) and EU FEDER (project MAT2010-20537) and the PAI of the Regional Government of Andalucía (project P10-FQM-6462). J.J.I. acknowledges a research contract from the Regional Government of Andalucía.

Journal of Alloys and Compounds, 553 (2013) 119-124
http://dx.doi.org/10.1016/j.jallcom.2012.11.099

Table 1. DSC peak temperatures corresponding to first (1) and second (2) exothermic processes.

Milling time [h]	c-B sample		a-B sample	
	$T_X(1)$ [K]	$T_X(2)$ [K]	$T_X(1)$ [K]	$T_X(2)$ [K]
4			732	854
6	769		731	852
10	756		733	836
20	748		726	849
30	740	859	726	850
40	738	858	728	848

Journal of Alloys and Compounds, 553 (2013) 119-124
http://dx.doi.org/10.1016/j.jallcom.2012.11.099

Figure caption

Figure 1. XRD patterns for crystalline (above) and commercial amorphous (below) boron powders used to prepare the initial mixtures.

Figure 2. XRD patterns at selected milling times for the three studied alloys.

Figure 3. Fraction of the bcc-Nb phase as a function of milling time.

Figure 4. Mössbauer spectra and hyperfine field distribution at some selected milling times for the three studied alloys.

Figure 5. (a) HAADF image, (b) SAED pattern of the amorphous matrix (the position of the (110) line of bcc-Fe type phase calculated from XRD results is indicated for reference) and (c) SAED pattern of a boron inclusion in [110] zone axis (inset shows the indexation in a arbitrary scale for clarity) for a-B alloy after 40 h milling.

Figure 6. EDX and EELS line profiles (line is shown in the image) for a-B alloy after 40 h milling.

Figure 7. EELS spectra after subtraction of the background showing the B K-edge for a-B alloy on a boron inclusion and on the matrix, respectively.

Figure 8. DSC scans at selected milling times for the three studied alloys.

Figure 9. Evolution of (a) lattice parameter, (b) crystal size and (c) microstrains as a function of milling time for bcc-Fe(NbB) phase.

Figure 10. Milling time dependence of (a) crystal volume fraction and (b) Fe fraction in

HF≤ 5 T sites. (c) Isomer shift corresponding to Fe fraction in HF ≤5T sites.

Journal of Alloys and Compounds, 553 (2013) 119-124
http://dx.doi.org/10.1016/j.jallcom.2012.11.099

Figure 1.

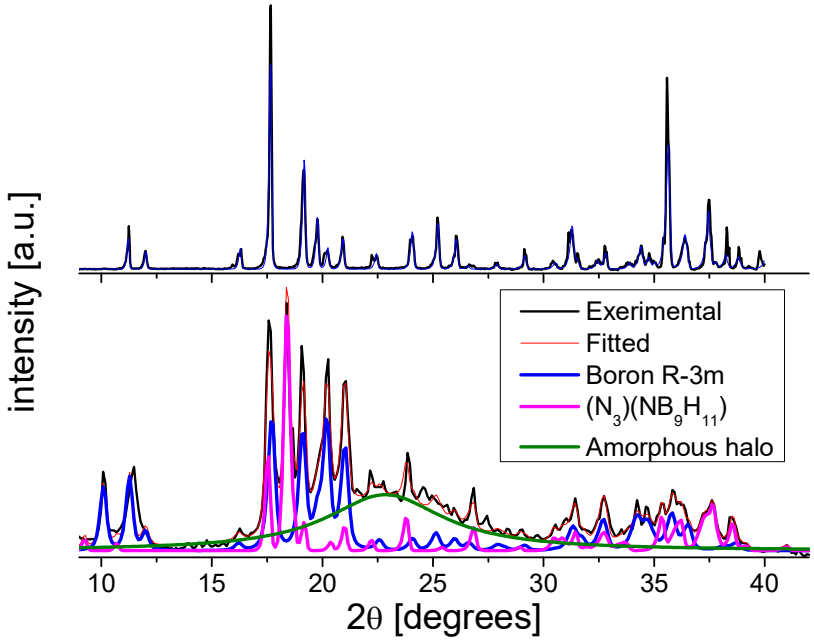

Journal of Alloys and Compounds, 553 (2013) 119-124
http://dx.doi.org/10.1016/j.jallcom.2012.11.099

Figure 2.

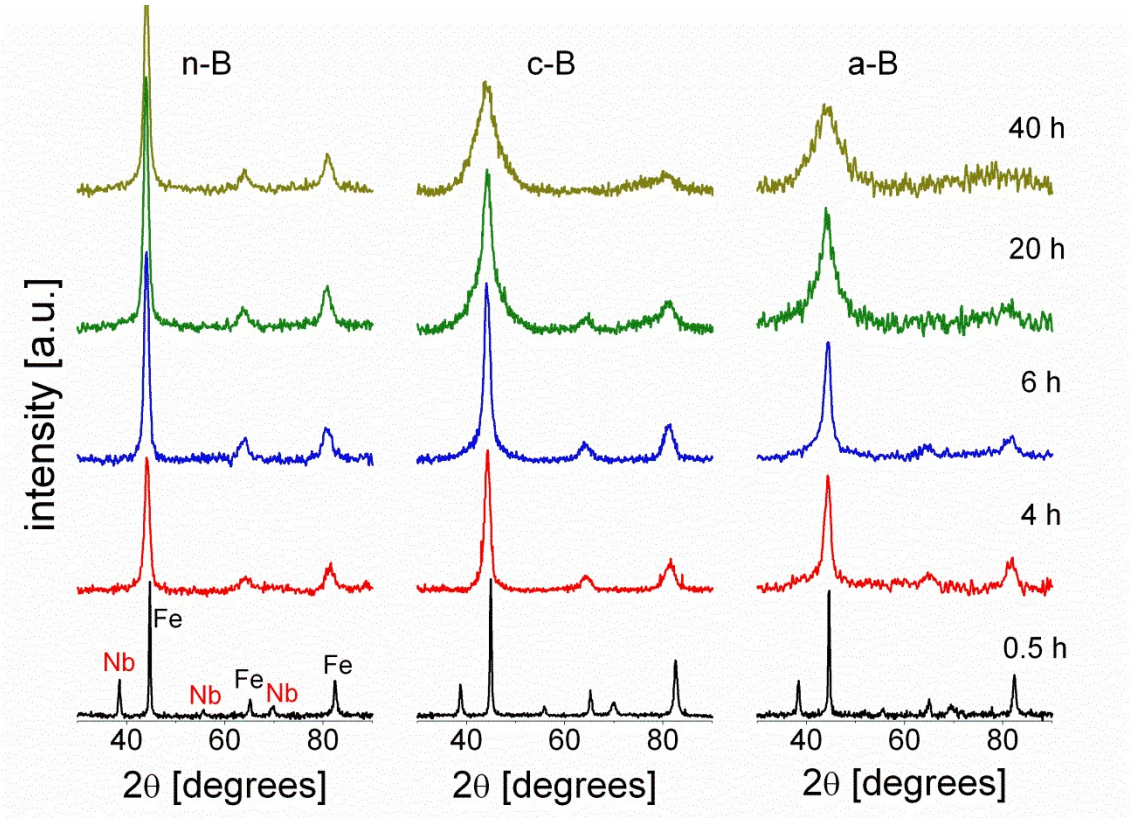

Journal of Alloys and Compounds, 553 (2013) 119-124
http://dx.doi.org/10.1016/j.jallcom.2012.11.099

Figure 3.

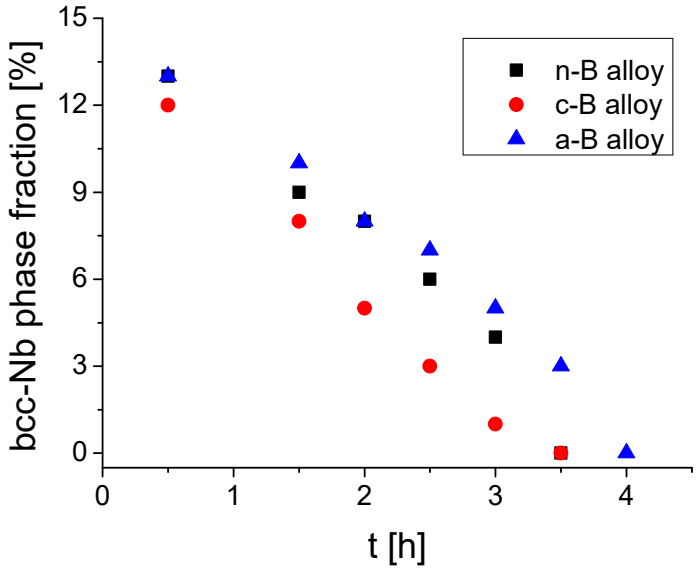

Journal of Alloys and Compounds, 553 (2013) 119-124
http://dx.doi.org/10.1016/j.jallcom.2012.11.099

Figure 4.

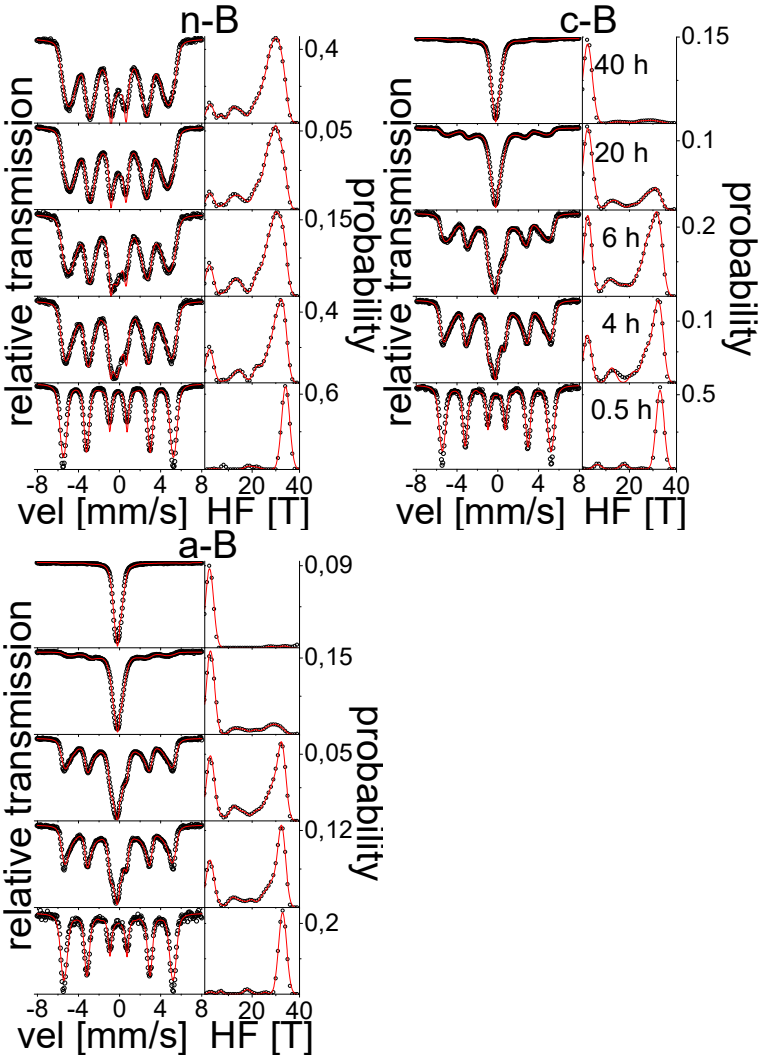

Journal of Alloys and Compounds, 553 (2013) 119-124
http://dx.doi.org/10.1016/j.jallcom.2012.11.099

Figure 5.

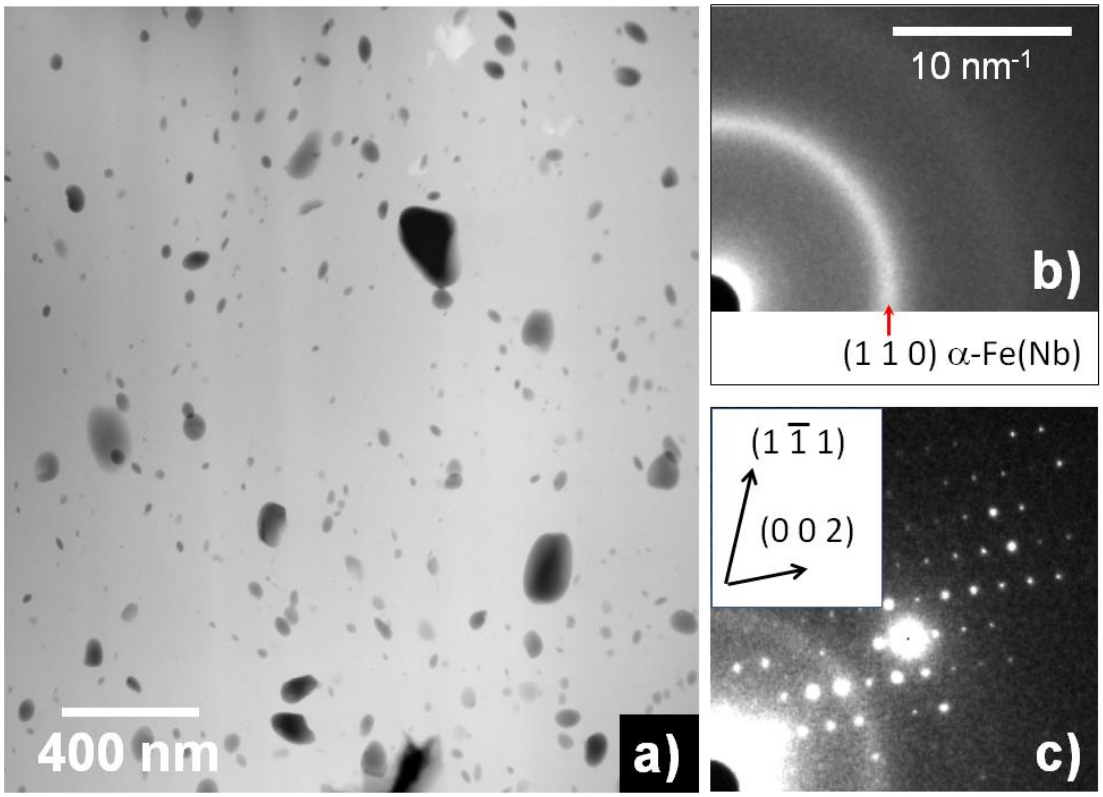

Journal of Alloys and Compounds, 553 (2013) 119-124
http://dx.doi.org/10.1016/j.jallcom.2012.11.099

Figure 6.

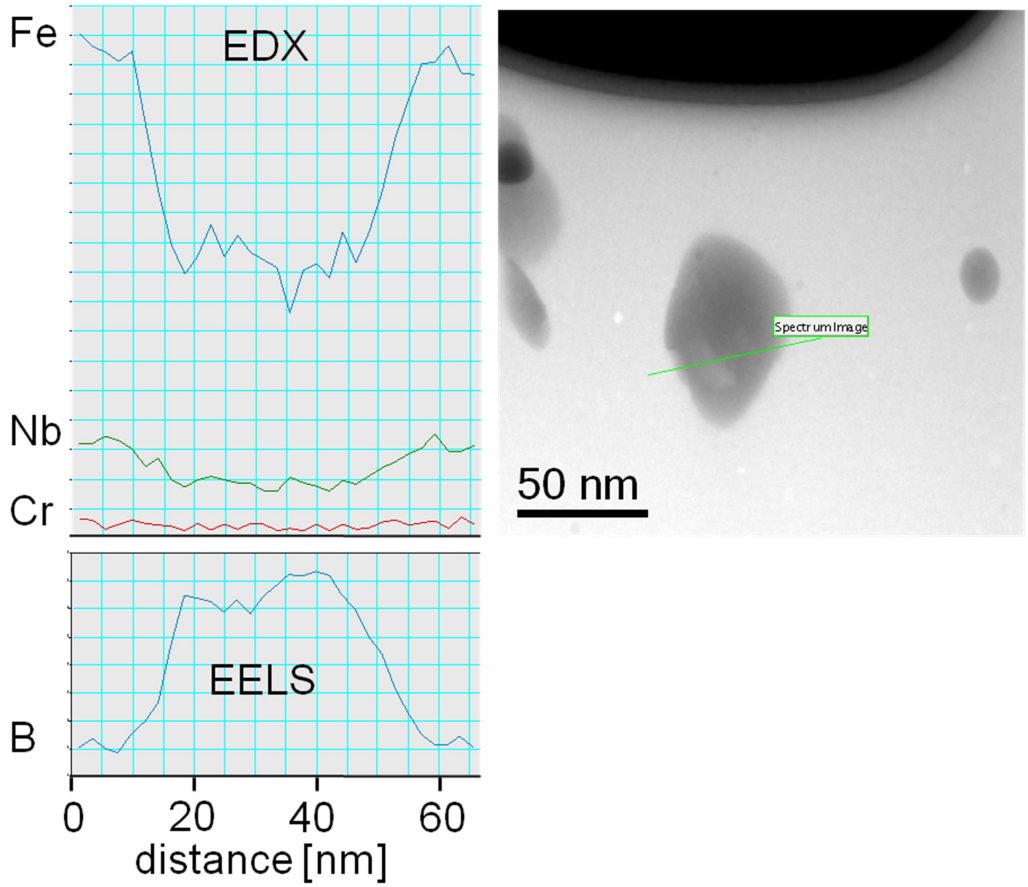

Journal of Alloys and Compounds, 553 (2013) 119-124
http://dx.doi.org/10.1016/j.jallcom.2012.11.099

Figure 7.

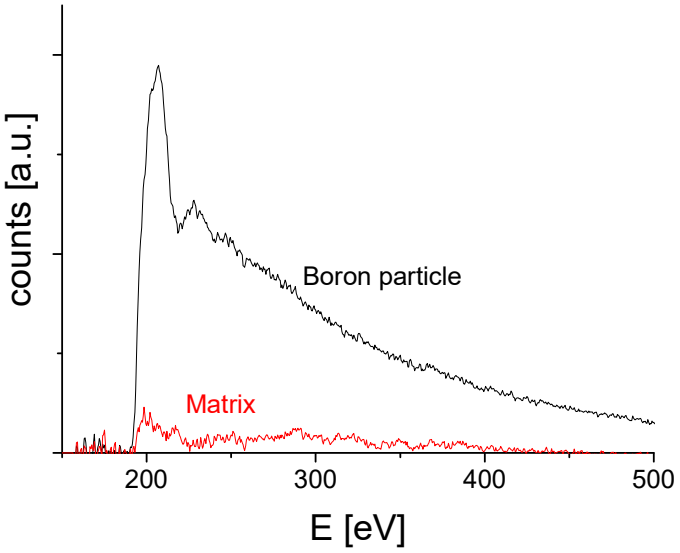

Journal of Alloys and Compounds, 553 (2013) 119-124
http://dx.doi.org/10.1016/j.jallcom.2012.11.099

Figure 8.

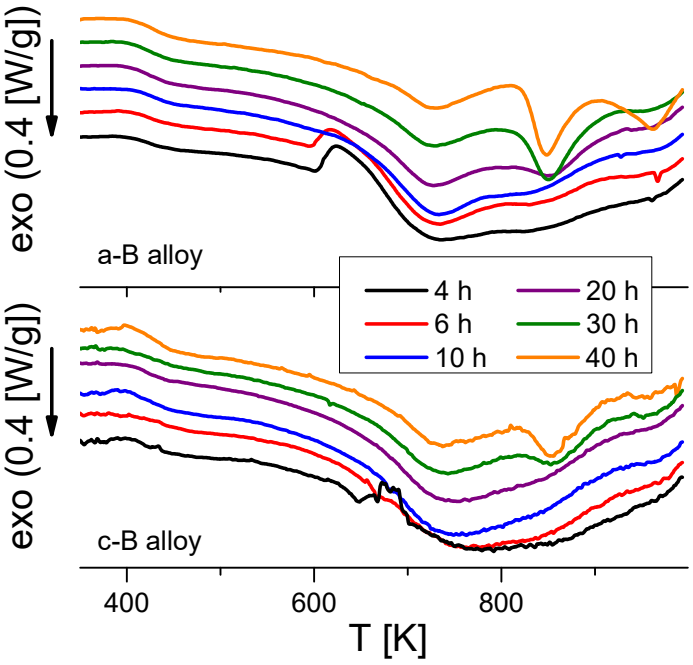

Journal of Alloys and Compounds, 553 (2013) 119-124
http://dx.doi.org/10.1016/j.jallcom.2012.11.099

Figure 9.

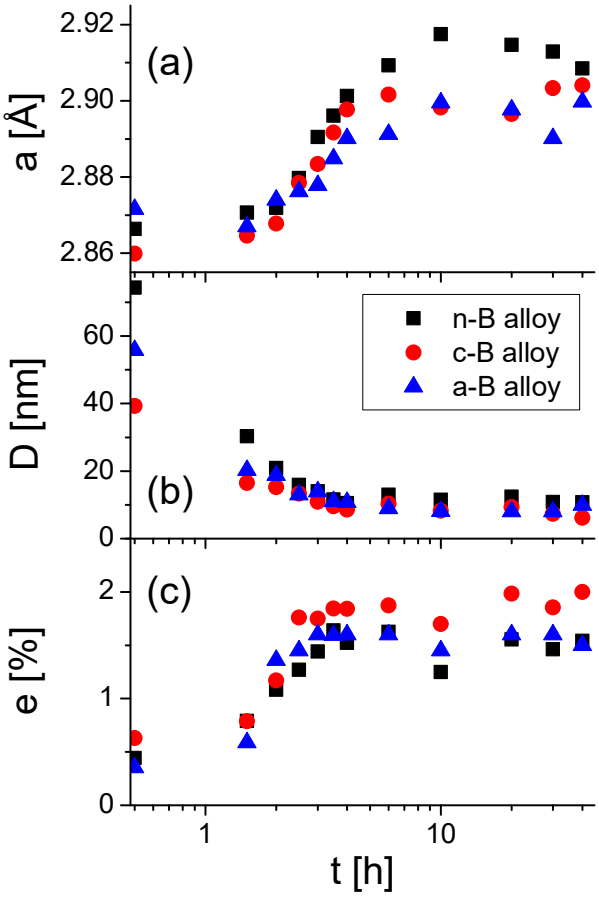

Journal of Alloys and Compounds, 553 (2013) 119-124
http://dx.doi.org/10.1016/j.jallcom.2012.11.099

Figure 10.

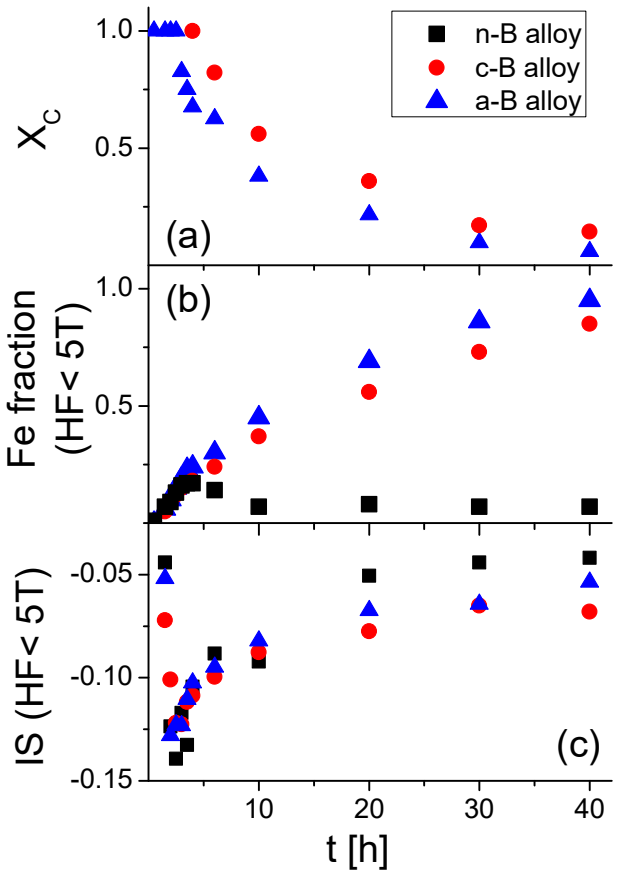

References

[1] M.E. McHenry, M.A. Willard, D.E. Laughling, Prog. Mater. Sci. 44 (1999) 291-433.

[2] K. Suzuki, N. Kataoka, A. Inoue, A. Makino, T. Matsumoto, Mater. Trans. JIM 31 (1990) 743-746.

[3] A. Makino, T. Hatanai, A. Inoue, T. Matsumoto, Mater. Sci. Eng. A 226-228 (1997) 594-602.

[4] A. Hernando, M. Vazquez, T. Kulik, C. Prados, Phys. Rev. B 51 (1995) 3581-3586.

[5] I. Chicinas, N. Jumate, G. Matei, J. Magn. Magn. Mater. 140-144 (1995) 1875-1876.

[6] C. Suryanarayana, Prog. Mater. Sci. 46 (2001) 1-184.

[7] J.J. Ipus, J.S. Blázquez, V. Franco, A. Conde, Intermetallics 16 (2008) 1073-1082.

[8] J.J. Ipus, J.S. Blázquez, S. Lozano-Perez, A. Conde, Philos. Mag. 89 (2009) 1415-1423.

[9] R. A. Brand, J. Lauer, D. M. Herlach, J. Phys. F: Met. Phys. 13 (1983) 675-683.

[10] S. Lozano-Pérez, Micron 39 (2008) 320.

[11] J. M. Greneche, A. Slawska-Waniewska, J. Magn. Magn. Mater. 215-216 (2000) 264-267.

[12] J.S. Blázquez, J.J. Ipus, M. Millán, V. Franco, A. conde, D. Oleszak, T. Kullik, J. All. Comp. 469 (2009) 169-178.

[13] E. Jartych, D. Oleszak and J.K. Zurawicz, Hyp. Int. 136 (2001) 25-33.

[14] J.Y. Yang, T.J. Zhang, K. Cui, X.G. Li, J. Zhang, J. All. Comp. 242 (1996) 153-156.

[15] J.S. Blázquez, J.J. Ipus, C.F. Conde, A. Conde, J. All. Comp. 536S (2012) 9-12.

[16] P. Butyagin, J. Mater. Synth. Proc. 8 (2000) 205-211.

[17] J.J. Ipus, J.S. Blázquez, V. Franco, M. Millán, A. Conde, D. Oleszak, T. Kulik, Intermetallics 16 (2009) 470-478.

[18] A. Blanchowski, K. Ruebenbauer, J. Zukrowski, Phys. Stat. Sol. (b) 15 (2005) 3201-3208.